Quantum phase transitions in effective spin-ladder models for graphene zigzag nanoribbons

Cornelie Koop and Stefan Wessel

Institut für Theoretische Festkörperphysik, JARA-FIT and JARA-HPC, RWTH Aachen University, 52056 Aachen, Germany
(Received 26 July 2017; published 9 October 2017)

We examine the magnetic correlations in quantum spin models that were derived recently as effective low-energy theories for electronic correlation effects on the edge states of graphene nanoribbons. For this purpose, we employ quantum Monte Carlo simulations to access the large-distance properties, accounting for quantum fluctuations beyond mean-field-theory approaches to edge magnetism. For certain chiral nanoribbons, antiferromagnetic interedge couplings were previously found to induce a gapped quantum disordered ground state of the effective spin model. We find that the extended nature of the intraedge couplings in the effective spin model for zigzag nanoribbons leads to a quantum phase transition at a large, finite value of the interedge coupling. This quantum critical point separates the quantum disordered region from a gapless phase of stable edge magnetism at weak intraedge coupling, which includes the ground states of spin-ladder models for wide zigzag nanoribbons. To study the quantum critical behavior, the effective spin model can be related to a model of two antiferromagnetically coupled Haldane-Shastry spin-half chains with long-ranged ferromagnetic intrachain couplings. The results for the critical exponents are compared also to several recent renormalization-group calculations for related long-ranged interacting quantum systems.

I. INTRODUCTION

Graphene-based nanoribbons with zigzag edge termination are characterized by the presence of an almost flat band of edge states [1]. The corresponding strongly increased local density of states allows electron-electron interactions to induce enhanced magnetic correlations along the edges, as compared to bulk graphene [2]. In fact, from a broad range of theoretical studies, a general picture has been promoted that the edge states along each edge of the zigzag nanoribbon are gapped out and exhibit a ferromagnetic alignment, thereby forming a pair of edge superspins that are correlated antiferromagnetically across the nanoribbon's transverse extent [3–10]. Even though recent progress in synthesizing graphene zigzag nanoribbons and controlling the edge alignment allows us to identify and better characterize the localized edge states [11–14], a fully conclusive experimental demonstration of such edge magnetism is still not generally agreed upon.

The above picture is aggravated by the fact that even within the most simple theoretical approach to edge magnetism, based on a local Hubbard model tight-binding description of graphene nanoribbons, it has been argued that quantum fluctuations, which are neglected in most mean-field-theory based predictions of the edge magnetism, suppress the ferromagnetic correlations along the nanoribbon edges [15–19]. For the case of specific chiral nanoribbons, where zigzag-terminated edge segments are separated by armchair-terminated steps, it was also shown within effective quantum spin models for the magnetic correlations [20,21] that the antiferromagnetic interedge coupling leads to a quantum disordered state, characterized by an exponential decay of the magnetic correlations along the edges and a finite spin excitation gap [19].

The effective quantum spin models referred to above can be derived from the parent Hamiltonian (the Hubbard model on the nanoribbon lattice) via a sequence of controlled approximations that separate on the microscopic level the edge states from the bulk states of the nanoribbon in an optimized Wannier basis (for details on the derivation of the effective spin model, and the extension to a second-order treatment within the Schrieffer-Wolff transformation, we refer to Refs. [20,21]). These effective theories are formulated in terms of a spin-half Heisenberg model, and the corresponding lattice geometry is that of an effective two-leg ladder with extended ferromagnetic exchange interactions along the legs (each representing one of the nanoribbon edges) and extended antiferromagnetic interactions between spins on different legs. While the general form of such spin-ladder models for graphene nanoribbons has been described previously [3,6,22], the calculations in Refs. [20,21] provide a systematic way to evaluate the effective exchange couplings for a given specific microscopic nanoribbon geometry.

A useful aspect of such effective spin-ladder models is the fact that they allow us to probe long-ranged magnetic correlations on significantly larger length scales than those accessible to direct simulations [18] of the parent Hamiltonian for chiral nanoribbons in terms of the Hubbard model, so that even large finite correlation lengths can be quantified [19]. For the chiral ribbons considered in Ref. [19], the interactions in the effective spin-ladder model decay exponentially with the spatial distance between the spins. The effective two-leg ladder model therefore behaves qualitatively similar to a two-leg ladder Heisenberg model with only nearest-neighbor ferromagnetic leg coupling and antiferromagnetic rung coupling: any finite value of the rung coupling results in a gapped quantum disordered state from the formation of dominant rung singlets [23–25]. For the effective spin models with extended interactions, the singlets of the spin gapped state extend over larger spatial regions, quantified by the correlation length [19].

Returning to pure zigzag nanoribbons, it was recently shown [21] that similarly to the chiral case, effective quantum spin models with a two-leg ladder geometry can also be derived for the case of wide zigzag nanoribbons, starting from the Hubbard model description; cf. the inset of Fig. 1 for an illustration. In contrast to the case of the chiral nanoribbons, however, these effective spin models have not been further analyzed with respect to their magnetic properties.
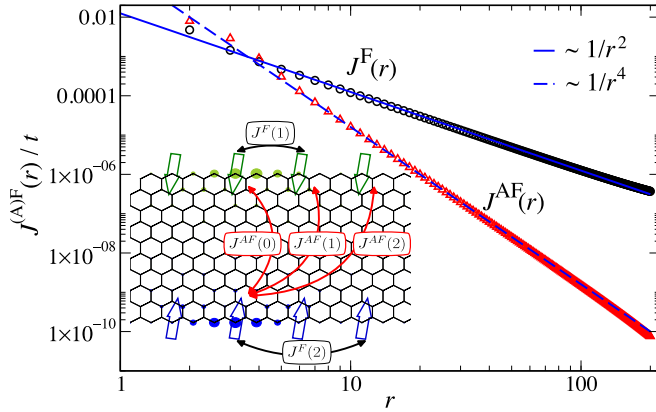
FIG. 1. Effective ferromagnetic $[J^{\mathrm{F}}(r)]$ and antiferromagnetic $[J^{\mathrm{AF}}(r)]$ couplings for a $W = 10$ zigzag nanoribbon for the Hubbard model parameters $U = t$ as a function of the lateral distance r. To calculate these effective coupling parameters, a finite-size ribbon with $W = 10$ zigzag lines and a total of 48 000 lattice sites was considered. The resulting values for the couplings of distances $r \leqslant 4$ are given explicitly in Table I. The inset illustrates a $W = 10$ zigzag nanoribbon along with some of the effective exchange interactions of the effective spin-ladder models in terms of the edge magnetic moments. Circles represent the amplitude of the Wannier functions corresponding to two of these edge states on the nanoribbon sites (one shown on the upper, and one on the lower edge).

Here, we study these effective spin-ladder models for zigzag nanoribbons using large-scale quantum Monte Carlo simulations [19,26,27]. This allows us to account within the effective quantum spin model for quantum fluctuations beyond mean-field theory, while we can also access the large-distance correlations. As will be discussed in detail below, the effective spin models for the zigzag nanoribbons exhibit a relatively weak spatial decay of the intraedge spin-spin interactions. More specifically, as a function of the lateral distance r between two spins, the numerically determined values of the ferromagnetic intraedge exchange interactions fit well to a power-law asymptotic decay proportional to $1/r^2$, while the antiferromagnetic interedge interactions decay faster, approximately proportional to $1/r^4$ at large values of r. This results in a qualitatively different magnetic behavior as compared to the chiral case [19]: we find that the quantum disordered region, which characterized the ground state of the effective quantum spin model for chiral ribbons, is reached in the case of the zigzag effective spin model only upon further increasing the antiferromagnetic interedge coupling strength beyond a finite critical value, which defines a quantum critical point at a rather large value of the interedge coupling strength.

We determine the critical scaling properties at this quantum critical point explicitly for a simplified version of the effective spin model, wherein the antiferromagnetic interedge coupling is truncated beyond its nearest-neighbor term. In fact, this more genuine quantum spin model can be seen as a basic spin model of two antiferromagnetically coupled ferromagnetic Haldane-Shastry spin-half chains [28–30]. A single ferromagnetic Haldane-Shastry chain has a ferromagnetic ground state, and its thermodynamic properties have been obtained within a well-known exact solution [30]. In this paper, we

show that the system of two antiferromagnetically coupled Haldane-Shastry chains features a quantum phase transition between a low-coupling gapless phase and a strong-coupling quantum disordered region where dominant singlets form along the interchain bonds. We determine numerically the critical properties of the quantum critical point that separates these two phases, and we compare our estimates for the critical scaling exponents to recent predictions based on renormalization-group (RG) calculations performed in the context of critical O(3) ϕ^4 theories, quantum rotor models, and quantum nonlinear σ models with power-law interactions [31–33]. We observe good overall agreement between our numerically extracted values for the critical exponents and the RG findings, adding further support to the identification of the quantum phase transition in the effective spin model from identifying its universal properties.

The outline of the rest of this paper is as follows: In Sec. II, we define in more detail the effective quantum spin model that we consider in our analysis, as well as the quantum Monte Carlo approach that we use. We present our results for the phase diagram and the properties of the quantum critical point in Sec. III, and finally we provide a discussion of our numerical findings and the relation to graphene zigzag nanoribbons in Sec. IV.

II. MODEL AND METHOD

In the following, we consider the effective quantum spin model for zigzag nanoribbons derived in Refs. [20,21], which maps onto a spin-half Heisenberg model on a two-leg ladder, described by the Hamiltonian

$$H = -\sum_{i,j} J_{ij}^{\mathrm{F}} \left(\mathbf{S}_{i,1} \cdot \mathbf{S}_{j,1} + \mathbf{S}_{i,2} \cdot \mathbf{S}_{j,2} \right)$$
$$+ \sum_{i,j} J_{ij}^{\mathrm{AF}} \, \mathbf{S}_{i,1} \cdot \mathbf{S}_{j,2}, \tag{1}$$

where $\mathbf{S}_{i,\mu}$ denotes a spin on the ith rung of the two-leg ladder, which for $\mu = 1$ (2) is located on the upper (lower) leg. Furthermore, $J_{ij}^{\mathrm{F}} > 0$ denotes the magnitude of the ferromagnetic exchange interaction for spins located on the same leg, and $J_{ij}^{\mathrm{AF}} > 0$ is the antiferromagnetic coupling between spins on different legs. Due to translational symmetry, these couplings depend only on the lateral distance $r_{ij} = |i - j|$, i.e., $J_{ij}^{\mathrm{(A)F}} = J^{\mathrm{(A)F}}(r_{ij})$. The actual values of the coupling constants, obtained as described in Refs. [20,21], depend explicitly on the physical parameters of the zigzag nanoribbon within the Hubbard model description. To leading order, the ferromagnetic couplings scale proportional to the local Hubbard repulsion U, and the antiferromagnetic couplings scale with t^2/U, where t denotes the nearest-neighbor hopping strength. For concreteness, we consider here the case in which $U = t$, well within the semimetallic region for the Hubbard model on a honeycomb lattice, in accord with the conditions in bulk graphene [2]. In the following, we consider a zigzag nanoribbon that is sufficiently wide, such that the edge magnetic moments are well described within the Wannier function basis [20,21]. We thus choose explicitly a zigzag nanoribbon with $W = 10$ zigzag lines (cf. the inset of Fig. 1 for an illustration), for which we obtained the effective coupling

TABLE I. Values of the spin exchange couplings for lateral distances $r \leqslant 4$, as obtained for the effective spin-ladder model for the $W = 10$ nanoribbon for $U = t$.

r	$J^{\mathrm{F}}(r)/t$	$J^{\mathrm{AF}}(r)/t$
0		0.0196417
1	0.0453914	0.0155852
2	0.0047475	0.0079814
3	0.0014386	0.0028894
4	0.0007365	0.0008942

strengths given in the main panel of Fig. 1 as well as, for $r \leqslant 4$, in Table I. These are based on a calculation for a $W = 10$ nanoribbon with 48 000 lattice sites. Furthermore, from comparing the results for $W = 10$ zigzag nanoribbons of varying sizes, we ensured that the shown values of the effective couplings are not affected by finite-size effects.

The log-log plot in Fig. 1 exhibits an essentially algebraic decay of the calculated exchange couplings as a function of distance for values of $r \gtrsim 5$, traced over several orders of magnitude in the interaction strength. As indicated by the corresponding fit lines, this large-r behavior is captured reasonably well in terms of asymptotic algebraic decays $J^{\mathrm{F}}(r) \propto 1/r^2$ and $J^{\mathrm{AF}}(r) \propto 1/r^4$, respectively. Fitting the couplings to power-law decays, one obtains estimated exponents of 1.94 and 4.09, respectively. Given the approximate nature of the coupling constant calculation, we prefer to employ for further analysis the very close and more natural values of 2 and 4, respectively. We considered also other values of the nanoribbon width, $W = 8$ and 12, and also for these ribbons the above asymptotic algebraic decays do fit the numerical results similarly well. Based on these algebraic forms, we can thus use the following explicit form of the longer-ranged coupling constants in the Hamiltonian H:

$$J^{\mathrm{F}}(r) = J_{\mathrm{F}} \frac{1}{r^2}, \quad J^{\mathrm{AF}}(r) = J_{\mathrm{AF}} \frac{1}{r^4}, \quad r > 4, \quad (2)$$

with the fit parameters $J_{\mathrm{F}}/t = 0.010\,09$ and $J_{\mathrm{AF}}/t = 0.219\,72$, while for smaller distances, the values of the interactions for $W = 10$ are given explicitly in Table I.

To systematically study the physics of the Hamiltonian H with the above form of the couplings, it is instructive to tune the relative strength of the interleg to intraleg couplings beyond these original values. For this purpose, we introduce a dimensionless quantity λ, which uniformly rescales all the interleg couplings as

$$J^{\mathrm{AF}}(r) \rightarrow \lambda J^{\mathrm{AF}}(r). \quad (3)$$

Hence, for $\lambda = 1$ we recover the original model, while for larger λ we (artificially) enhance all antiferromagnetic interleg couplings with respect to the ferromagnetic intraleg couplings. As will be demonstrated in the next section, the Hamiltonian H indeed exhibits a quantum phase transition upon varying the parameter λ, which we referred to already.

Furthermore, we find that the basic physics of the Hamiltonian H is reproduced also for a simplified model Hamiltonian, which is obtained by truncating the antiferromagnetic exchange couplings beyond the nearest-neighbor term and using a simple $1/r^2$ decay for all ferromagnetic couplings

$r \geqslant 1$. This leads us to an even more genuine spin model with Hamiltonian

$$\tilde{H} = -J_F \sum_{i,j} \frac{1}{r_{ij}^2} (\mathbf{S}_{i,1} \cdot \mathbf{S}_{j,1} + \mathbf{S}_{i,2} \cdot \mathbf{S}_{j,2})$$

$$+ J_{\mathrm{AF}} \sum_i \mathbf{S}_{i,1} \cdot \mathbf{S}_{i,2}. \quad (4)$$

For this model, we furthermore define the ratio

$$g = \frac{J_{\mathrm{AF}}}{J_F} \quad (5)$$

between the two coupling parameters. Similarly to the parameter λ in the Hamiltonian H, g quantifies for the Hamiltonian $\tilde{H}$ the relative strength of the antiferromagnetic interleg coupling with respect to the ferromagnetic intraleg coupling strength.

In the limit of $J_{\mathrm{AF}} = 0$ (i.e., $g = 0$), this model corresponds to two decoupled spin chains with a ferromagnetic $1/r^2$ exchange interaction. In the thermodynamic limit, this is the ferromagnetic Haldane-Shastry model for which an exact solution has been derived for its thermodynamic properties [28–30]. This model has a fully polarized, ferromagnetic ground state. Given the short-ranged character of the interleg coupling in $\tilde{H}$, we expect in this case a quantum disordered phase from the formation of strong rung-singlets in the opposite limit of large J_{AF}, i.e., for $g \rightarrow \infty$, along with a finite spin excitation gap. Note that due to the explicit ferromagnetic $1/r^2$ coupling between any two spins within a given leg, the correlation function decays proportional to $1/r^2$ even deep inside the quantum disordered region, as one also finds explicitly within perturbation theory about the large-g limit.

Any finite value of the antiferromagnetic rung coupling, $g > 0$, tends to lock the spins between the two legs into an antiferromagnetic alignment. However, in contrast to the case of a purely short-ranged intraleg coupling [23–25], this locking does not immediately destroy the ferromagnetic state along each leg due to the long-ranged character of the intraleg coupling. Instead, as demonstrated in the next section, a quantum phase transition emerges at a finite value of $g > 0$, which separates the weak coupling (low-g) from the strong coupling (large-g) phase. In this sense, the long-ranged character of the ferromagnetic intraleg coupling stabilizes the weak-coupling phase, in contrast to the case of the conventional two-leg ladder, where any finite rung coupling drives the system into the gapped rung-singlet regime.

Since for the Hamiltonian H the antiferromagnetic interleg coupling decays fast with the lateral distance (as compared to the intraleg couplings), this extended form of the interleg coupling does not modify the above picture. In fact, as we will show in the following section, also for H we can identify a quantum critical point at a finite value of λ. One may indeed expect this, recalling that quite generally in one-dimensional systems, power-law interactions decaying faster than $1/r^3$ lead to the same critical properties as short-ranged interactions.

Before we turn to the presentation of our results, we comment on the numerical approach that we used for our investigation. We analyzed the properties of the model Hamiltonians H and $\tilde{H}$ using quantum Monte Carlo (QMC) simulations. In fact, both models are free of geometric frustration, so that

no QMC sign problem occurs. To efficiently perform the QMC sampling in the presence of the long-ranged interactions, we used the stochastic series expansion QMC method for quantum spin systems with an efficient sampling scheme [26,27], similar to previous studies for the effective spin model for chiral nanoribbons [19]. In particular, we simulated finite two-leg ladder systems with the Hamiltonians H and $\tilde{H}$ using periodic boundary conditions (PBCs) along the lateral direction. To reduce the finite-size effects in the QMC simulations and access more efficiently the behavior of the effective spin models on large distances, we furthermore performed an Ewald summation of the long-ranged effective spin interactions [27]. For a given pair of spins with lateral distance r, we thus replace the coupling constant for the finite system with L rungs (i.e., L spins on each leg of the two-leg ladder, and a total of $N = 2L$ spins) by a summation over all replica-repeated images. In particular, for the ferromagnetic couplings in $\tilde{H}$, we obtain a closed form, since the Ewald summation leads to

$$\frac{J_F}{r^2} \longrightarrow \sum_{k=-\infty}^{\infty} \frac{J_F}{(r - kL)^2} = J_F \frac{\pi^2/L^2}{\sin^2\left(\frac{r\pi}{L}\right)} = \frac{J_F}{\zeta(r)^2}, \quad (6)$$

where the closed form of the above series can be found, e.g., in Ref. [27], and we defined

$$\zeta(r) = \sin(r\,\pi/L)L/\pi. \quad (7)$$

One may notice that the above closed form of the ferromagnetic coupling for PBCs is also usually considered in the Haldane-Shastry model for finite chains, and in fact, $\zeta(r_{ij}) = \sin(r_{ij}\,\pi/L)L/\pi$ equals the chord distance for a periodic chain with L sites between lattice sites i and j. In the context of conformal field theory, ζ is often called the conformal distance (or length), and we will also use this notation further below. For the couplings in the Hamiltonian H, we also performed a corresponding Ewald summation, for which, however, we do not obtain a closed form, and instead performed the summation numerically.

In the following section, we present our results from QMC simulations of both model Hamiltonians. Since our QMC method is a finite-temperature scheme, we monitor the behavior of various physical quantities in the low-temperature region in order to extract the ground-state behavior, considering system sizes with typically 20 000 and in some cases up to 32 000 quantum spin-half sites. Furthermore, we use units in the following such that the nearest-neighbor ferromagnetic intraleg coupling is set equal to 1, i.e., $J^F(r = 1) = 1$ for H and $J_F = 1$ for $\tilde{H}$, respectively. In addition, we use $k_B = 1$.

III. RESULTS

In the following subsection, we show that both models H and $\tilde{H}$ feature a quantum phase transition between a gapless phase at weak interleg coupling and the gapped, quantum disordered phase for strong interleg couplings. In the next subsection, we then analyze the scaling behavior at the quantum critical point, focusing on the more genuine Hamiltonian $\tilde{H}$, and we compare our results to recent RG calculations on related quantum systems.

A. Quantum phase transition

In the absence of any interleg coupling, both models consist of two decoupled ferromagnetic Haldane-Shastry chains [28–30], and each chain has a long-range-ordered ferromagnetic ground state. At any finite temperature T, this ferromagnetic order is destroyed, with a correlation length that increases exponentially upon decreasing T. Correspondingly, an isolated ferromagnetic Haldane-Shastry chain exhibits an exponential divergence of the magnetic susceptibility [30] upon lowering T. To probe the low-temperature behavior of the magnetic correlations within each leg of the coupled-chain systems, in the QMC simulations we measured the corresponding single-leg susceptibility

$$\chi_{\text{leg}} = \frac{1}{L} \int_0^{1/T} d\tau \, \langle M_{\text{leg}}(\tau) M_{\text{leg}}(0) \rangle, \quad (8)$$

where $M_{\text{leg}} = \sum_i S_{i,\mu}^z$ denotes the total magnetic moment of the spins on one of the legs, and where $\mu = 1$ or 2 can be chosen equally well (within the QMC simulations, we average over both cases in order to improve the statistics). The above Kubo integral quantifies the fluctuations of the single leg's magnetic moment, with τ denoting the imaginary-time evolution. Here, we employ the SU(2) symmetry of the quantum spin Hamiltonian in order to evaluate the magnetic correlations directly in the computational (S^z) basis. Physically, χ_{leg} quantifies the linear response in the leg's magnetic moment M_{leg} upon applying a uniform magnetic field along a single leg of the ladder.

The overall magnetic response of the two-leg ladder models is obtained from the uniform susceptibility

$$\chi_{\text{uni}} = \frac{1}{N} \int_0^{1/T} d\tau \, \langle M(\tau) M(0) \rangle = \frac{1}{TN} \langle M^2 \rangle, \quad (9)$$

in terms of the fluctuations in the total system's ($N = 2L$) magnetic moment $M = \sum_{i,\mu} S_{i,\mu}^z$. Note that while M commutes with both Hamiltonians, this is not the case for M_{leg} at any finite interleg coupling. In physical terms, χ_{uni} quantifies the linear response in the total magnetic moment M upon applying a uniform magnetic field to all the spins of the system.

In addition to the above quantities, one may also consider the overall system's staggered susceptibility

$$\chi_{\text{stag}} = \frac{1}{N} \int_0^{1/T} d\tau \, \langle M_{\text{stag}}(\tau) M_{\text{stag}}(0) \rangle, \quad (10)$$

where $M_{\text{stag}} = \sum_i (S_{i,1}^z - S_{i,2}^z)$. However, since $\chi_{\text{stag}} = 2\chi_{\text{leg}} - \chi_{\text{uni}}$, and (as we will also find from explicit calculations) $\chi_{\text{leg}} \gg \chi_{\text{uni}}$ at low temperatures due to the antiferromagnetic interleg coupling, χ_{stag} essentially probes the intraleg ferromagnetic response, which χ_{leg} accesses more directly. From the point of view of the edge magnetism, χ_{leg}, probing for ferromagnetic correlations within a single leg, may also appear to be the more natural quantity to consider.

We first consider the evolution of these quantities upon varying the parameter g for the Hamiltonian $\tilde{H}$. The left panel of Fig. 2 shows the low-temperature behavior of the single-leg susceptibility χ_{leg} for a system with $L = 8000$ and for different values of g in a region, where we observe a strong qualitative change in the low-T behavior. Namely, for values of $g < 1.95$, the single-leg susceptibility develops a strong
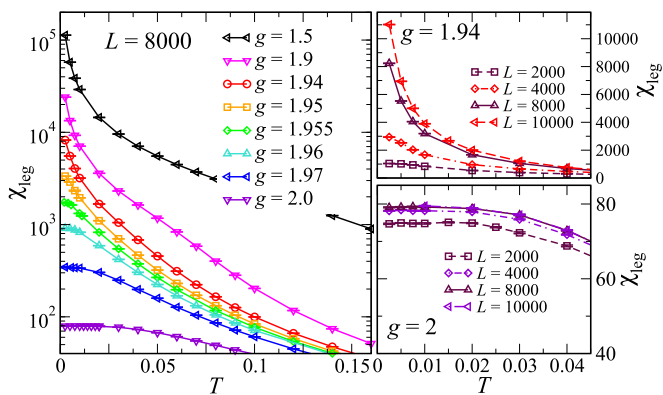
FIG. 2. Temperature dependence of the single-leg susceptibility χ_{leg} of the Hamiltonian $\tilde{H}$ for different values of g and for $L = 8000$ (left panel), and for different values of L at fixed $g = 1.94$ (upper right panel) and $g = 2$ (lower right panel).

divergence upon lowering T, similar to the case of an isolated ferromagnetic Haldane-Shastry model, while for values of $g > 1.96$ this divergence is suppressed at low temperatures, and χ_{leg} instead tends to a finite value for $T \to 0$. An exponential divergence of the magnetic susceptibility, such as that obtained for a single ferromagnetic Haldane-Shastry chain, is affected by finite-size effects in QMC simulations [34], so that in the low-temperature region, one needs to carefully monitor the behavior of the susceptibility upon varying the system size. This is shown for the two cases of $g = 1.94$ and 2 in the two right panels of Fig. 2. We find that for $g = 2$, the finite-size data show a convergent saturation in the low-temperature value of χ_{leg}, while the data for $g = 1.94$ show a steady increase upon increasing the system size. This rather drastic change in the low-temperature behavior of the single-leg response function upon a weak variation of the coupling ratio g by only a few percent is indicative of a quantum phase transition of the model within this parameter region.

We obtain further indication of a change in the ground-state properties from analyzing the uniform magnetic susceptibility χ_{uni}, for which our QMC results are shown in Fig. 3. From the temperature dependence of χ_{uni}, shown in the left panel of Fig. 3, we find for values of $g < 1.95$ a leading linear behavior
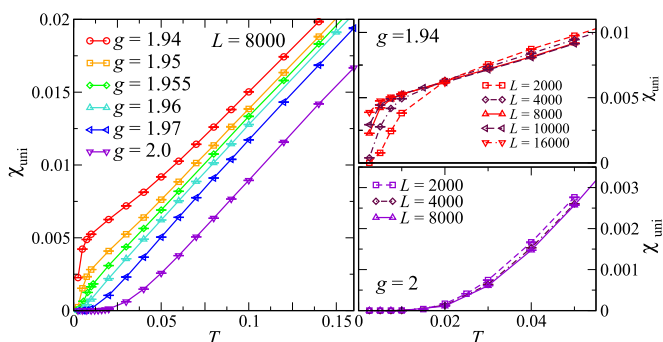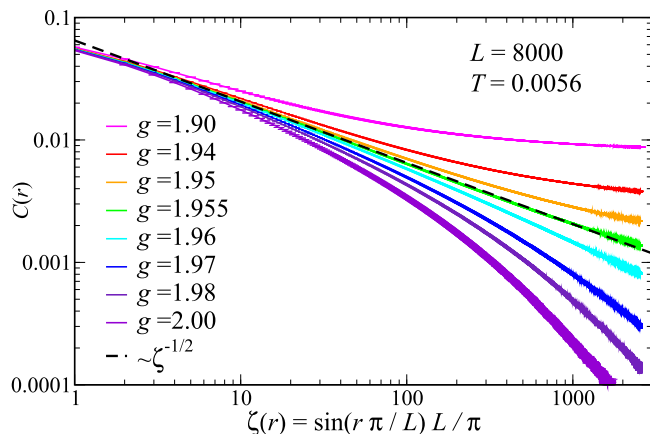

FIG. 3. Temperature dependence of the uniform susceptibility χ_{uni} of the Hamiltonian $\tilde{H}$ for different values of g and for $L = 8000$ (left panel), and for different values of L at fixed $g = 1.94$ (upper right panel) and $g = 2$ (lower right panel).

FIG. 4. Intraleg spin correlations $C(r)$ as a function of the conformal distance $\zeta(r) = \sin(r\,\pi/L)L/\pi$ for the Hamiltonian $\tilde{H}$ and for different values of g and for $L = 8000$ at $T = 0.0056$. The dashed line indicates a scaling proportional to $\zeta^{-1/2}$ near the quantum critical point.

that extrapolates to finite ground-state values. The sudden drop of χ_{uni} that sets in at very low temperatures is in fact a finite-size effect, as can be seen from a detailed view of the low-T behavior of χ_{uni} for different system sizes in the upper right panel of Fig. 3 for $g = 1.94$. In contrast, for $g > 1.96$, the low-temperature data show a strong suppression of the magnetic response χ_{uni}, which becomes more pronounced upon increasing the system size; cf. the lower right panel for $g = 2$. The finite-size effects for $g = 1.94$ (upper right panel) can also be distinguished from the low-T suppression of χ_{uni} for $g = 2$ (lower right panel) by a different curvature in the temperature dependence. Hence, similarly to the single-leg susceptibility, the uniform susceptibility exhibits a strong, qualitative change in the system's behavior in the vicinity of $g \approx 1.955$. Moreover, the vanishing uniform susceptibility for $g \gtrsim 1.955$ indicates the presence of a finite spin excitation gap Δ. In the next subsection, we will quantify the spin gap by extracting it from the low-temperature data for χ_{uni}, and we will also compare its dependence on the coupling ratio to predictions from scaling theory.

The above analysis of the thermodynamic response functions provides a strong indication of the presence of a quantum phase transition in the system described by $\tilde{H}$. To relate this observation more directly to the spin correlations within the legs of the coupled two-leg ladder system, we examine the correlation function

$$C(r_{ij}) = \left\langle S_{i,\mu}^z S_{j,\mu}^z \right\rangle \tag{11}$$

within a single leg ($\mu = 1$ or 2), which is shown as being obtained from QMC simulations on an $L = 8000$ system at a low temperature of $T = 0.0056$, and for different values of g within the transition region in Fig. 4. Here, we furthermore use the conformal distance $\zeta(r) = \sin(r\,\pi/L)L/\pi$ to quantify the lateral separation between the spins. We find again a qualitative change of the large-distance behavior of $C(r)$ at $g \approx 1.955$. For smaller values of g, the correlation function has a different curvature from the data for $g > 1.955$, which furthermore shows a strong suppression at large r. Moreover, the data for

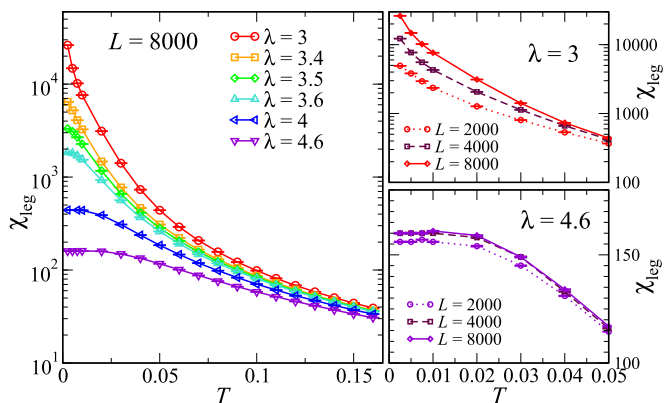FIG. 5. Temperature dependence of the single-leg susceptibility χ_{leg} of the Hamiltonian H for different values of λ and for $L = 8000$ (left panel), and for different values of L at fixed $\lambda = 3$ (upper right panel) and $\lambda = 4.6$ (lower right panel).

FIG. 6. Temperature dependence of the uniform susceptibility χ_{uni} of the Hamiltonian H for different values of λ and for $L = 8000$ (left panel), and for different values of L at fixed $\lambda = 2.05$ (upper right panel) and $\lambda = 2.1$ (lower right panel).

$g = 1.955$ compare well to an algebraic decay proportional to $\zeta^{-1/2}$, indicated by the dashed line in Fig. 4. Such an algebraic scaling behavior of the finite system's correlation function in terms of the conformal distance is characteristic of the decay of the correlation function at a quantum critical point, with an emerging conformal invariance in $(1 + 1)$-dimensional quantum systems. Note also that this slow algebraic decay is distinct from the asymptotic $1/r^2$ decay in the large-g region, which stems from the explicit ferromagnetic couplings decaying as $1/r^2$.

Summarizing these results, we have obtained an indication from both two-point correlation functions and global quantities that the Hamiltonian $\tilde{H}$ exhibits a quantum phase transition at $g \approx 1.955$ between a low-g gapless phase with long-ranged ferromagnetic correlations along each leg, and a large-g quantum disordered region with a finite spin excitation gap. Furthermore, an approximately algebraic decay of the correlation function is indicative of a quantum critical point, separating the two different phases. In the following subsection, we will confirm this basic observation by studying the properties of this quantum critical point within a more detailed finite-size scaling analysis.

Before we turn to this scaling analysis of the quantum critical point, we show that a similar behavior is also obtained for the Hamiltonian H, for which the interleg interactions have an extended $1/r^4$ decay, instead of the nearest-neighbor interleg coupling in $\tilde{H}$. In Figs. 5 and 6, we show our QMC results for χ_{leg} and χ_{uni} for the model Hamiltonian H. Indeed, we find a clear indication of a qualitative change in the system's properties upon increasing λ, and we estimate a critical coupling ratio of $\lambda_c \approx 3.4$. This value is consistent with the large distance behavior of the correlation function $C(r)$, shown in Fig. 7, which indicates a quantum critical point located at $\lambda_c \approx 3.425$. This plot also contains the correlation function $C(r)$ for $\lambda = 1$, and the corresponding data for the susceptibilities are shown in Fig. 8. The original effective spin-ladder model H for $\lambda = 1$ is thus localized well within the weak-coupling gapless phase with long-ranged ferromagnetic alignment along each leg stabilized in the ground state.
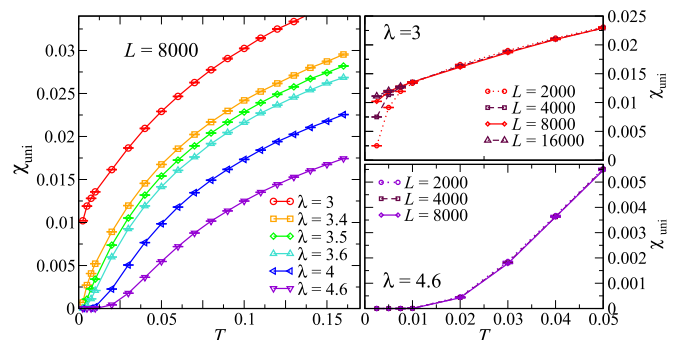
B. Quantum critical properties

To further examine the quantum phase transition in the effective quantum spin models, we analyze in this subsection its critical scaling properties, focusing for this purpose on the more genuine case of Hamiltonian $\tilde{H}$. It is convenient to first summarize some of the main findings from several recent RG studies of the quantum critical properties of related one-dimensional quantum systems with an O(3) symmetry in the presence of long-ranged interaction [31–33]. Some of these papers also consider the more general case of an O(n) symmetric interaction [31,33], while Ref. [32] focuses on the case of $n = 1$, which is relevant, e.g., for the quantum Ising model.

For a quantum system in 1+1 dimensions, with a spatially long-ranged interaction that decays proportional to $1/r^{1+\sigma}$ with the spatial distance r, such as an n-component quantum rotor model, the long-ranged nature of the interactions is important in order to stabilize a nontrivial transition. For example, short-ranged interacting quantum rotor models do
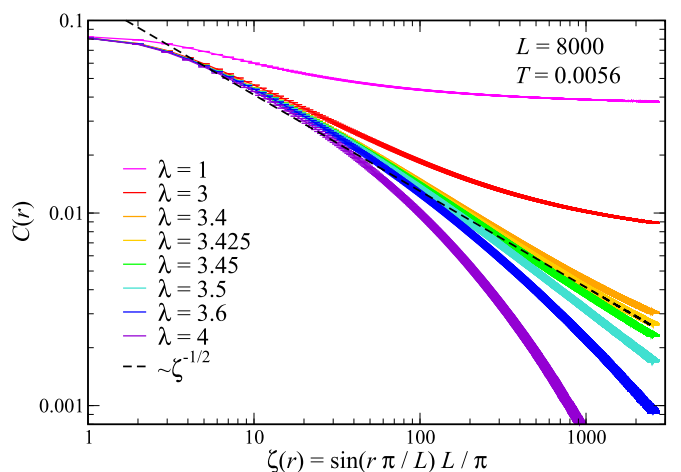

FIG. 7. Intraleg spin correlations $C(r)$ as a function of the conformal distance $\zeta(r) = \sin(r \pi/L)L/\pi$ for the Hamiltonian H and for different values of λ and for $L = 8000$ at $T = 0.0056$. The dashed line indicates a scaling proportional to $\zeta^{-1/2}$ near the quantum critical point.
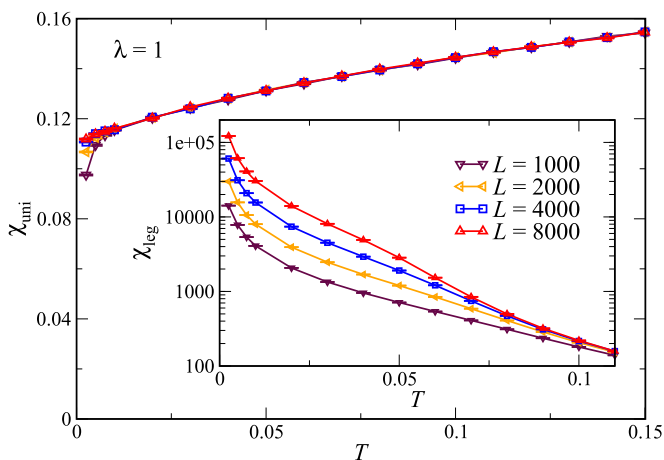
FIG. 8. Temperature dependence of the uniform susceptibility χ_{uni} (main panel) and the single-leg susceptibility χ_{leg} (inset) of the Hamiltonian H for $\lambda = 1$ for different values of L.

not exhibit quantum phase transitions for $n > 2$ in $1+1$ dimensions [31,35]. Of particular interest in the current discussion is the case $\sigma = 1, n = 3$. In the relevant region of σ (for $2/3 < \sigma < 2$), the critical exponents at the quantum phase transition differ from the mean-field values due to the effects of quantum fluctuations, and they have been approximately obtained as expansions in $\epsilon = 3\sigma/2 - d$ [31,32]. Here, d denotes the spatial dimension, and $3\sigma/2$ is indeed the upper critical dimension. In particular, within the ϵ expansion, Ref. [31] obtains from a one-loop calculation the result

$$\nu = \frac{1}{\sigma} + \frac{n+2}{n+8}\epsilon + O(\epsilon^2) \qquad (12)$$

for the critical exponent ν, which characterizes the divergence of the order parameter correlation length. Another recent work [32] reports $1/\nu = \sigma - \frac{\epsilon}{3} + O(\epsilon^2)$ for the special case of $n = 1$. This is in accord with the above result for $\sigma = 1$, the case of interest here, but differs from it in the general case (cf. Ref. [32] for further discussion). From Eq. (12), we thus obtain an estimate of $\nu \approx 1.227$ for $\sigma = 1$ and $n = 3$. Reference [32] furthermore reports a two-loop order result for the dynamical critical exponent z for $\sigma = 1, d < 2$ in the O(n) case,

$$z = \frac{1}{2} + \frac{(n+2)(12-\pi^2)}{16(n+8)^2}\tilde{\epsilon}^2 + O(\tilde{\epsilon}^3), \qquad (13)$$

where $\tilde{\epsilon} = 2 - d$, based on earlier RG calculations [36]. For the case of interest here ($d = 1$ and $n = 3$), this provides an estimate of $z \approx 0.505$. This value is also consistent with the RG results in Ref. [33]. It may be worthwhile to point out that within mean-field theory, a value of $z_{\text{MF}} = \sigma/2 < 1$ results for $\sigma < 2$, already reflecting the fact that due to the long-ranged nature of the spatial interactions, correlations in the temporal direction are weaker than in the spatial direction (in contrast to a dynamical critical exponent of 1, which is obtained for many quantum critical spin models with only short-ranged interactions) [31]. For $\sigma = 1$, this gives a mean-field value of $z_{\text{MF}} = 1/2$. With respect to the anomalous exponent η that characterizes the spatial decay of the order parameter correlation function $G(r)$ at the quantum critical point, different definitions are used in the literature. Here, we

follow the standard notation, with

$$G(r) \propto 1/r^{d+z-2+\eta} \qquad (14)$$

at criticality [35]. According to Refs. [31,33], the value of η in the relevant region of σ for our study is fixed to $\eta = 2 - \sigma$, so that for $d = \sigma = 1$ we obtain $G(r) \propto 1/r^z$. Again, for $d = \sigma = 1$, this form agrees with the findings in Ref. [32] (in their convention, $G(r) \propto 1/r^{d-1+\eta}$ and they obtain the relation $\eta = z$ for $\sigma = 1$ and $n = 1$). Another useful result reported in Refs. [31,32] for the case $\sigma = 1$ of interest here is the relation

$$\gamma/\nu = 1 \qquad (15)$$

between ν and the order parameter susceptibility exponent γ, which we can access in our model by the single-leg susceptibility χ_{leg}. Combined with the value of $\eta = 2 - \sigma$, this relation follows from the general scaling relation $\gamma = \nu(2 - \eta)$. In the following, we compare these RG results to our QMC estimates of the critical exponents, based on a finite-size scaling analysis of the numerical data.

For this purpose, we first briefly review the general finite-size scaling theory near a quantum critical point. In particular, for a quantity A that in the thermodynamic limit at $T = 0$ scales as $A \propto \delta g^{\phi_A}$ with the relative deviation $\delta g = |g - g_c|/g_c$ from the quantum critical point at g_c, the corresponding finite-size scaling form in the critical regime reads

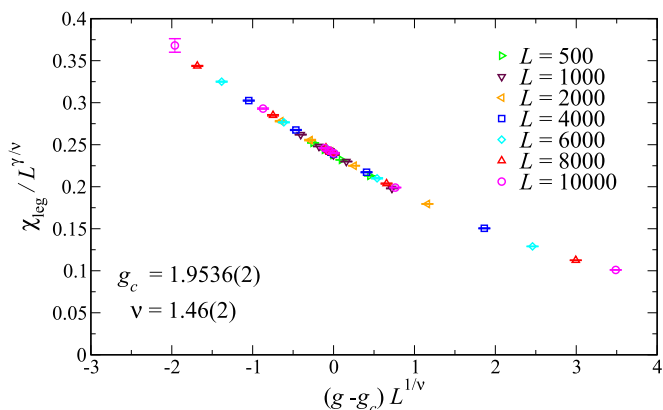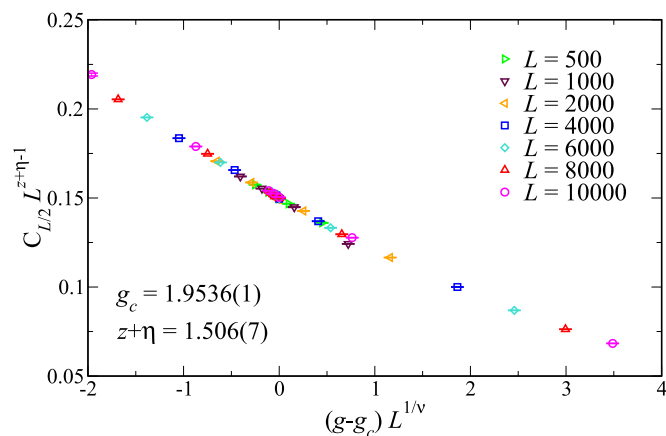$$A(L,T,g) \propto L^{-\phi_A/\nu} F_A(\delta g\, L^{1/\nu}, T L^z), \qquad (16)$$

in terms of a scaling function F_A. To probe the critical properties near g_c based on finite-temperature simulations, one performs low-temperature simulations for different system sizes L, scaling the inverse temperature $1/T \propto L^z$. One can then perform the scaling analysis in terms of a single scaling variable, since the second argument, $T L^z$, of F_A then takes on a constant value. Based on the above estimate for the dynamical critical exponent z, we set the simulation temperature to $T = T_L$, where T_L scales as $1/T_L = 2L^z$ in order to reach the quantum critical scaling regime near g_c (below we also determine an estimate of z that compares well to the RG predictions). From Eq. (16), we see that the rescaled data sets of $A(L,T_L,g)L^{\phi_A/\nu}$ for different system sizes L, when plotted as functions of g, exhibit a crossing point at $g = g_c$. Furthermore, one obtains a data collapse upon plotting the rescaled values of $A(L,T_L,g)L^{\phi_A/\nu}$ for different system sizes as functions of $\delta g\, L^{1/\nu}$ for g near g_c. These standard analysis techniques will now be used in order to estimate g_c as well as the critical exponents for the Hamiltonian $\tilde{H}$ in the following.

In our system, the order parameter quantifies the ferromagnetic alignment within each single leg, and the corresponding susceptibility is given in terms of the single-leg susceptibility χ_{leg}, which we examined already in the previous section. Here, we consider in more detail its finite-size scaling. Using the RG prediction of $\gamma/\nu = 1$, we indeed observe a crossing point in a plot of the rescaled finite-size data $\chi_{\text{leg}}/L^{\gamma/\nu}$ as a function of g, cf. Fig. 9. We observe a sharp crossing of the finite-size data for sufficiently large values of $L \geqslant 500$. Only the data for the smallest shown system size, $L = 100$, exhibit the presence of further corrections to scaling. This crossing plot allows us to obtain a refined value of $g_c \approx 1.9536$. Furthermore, from
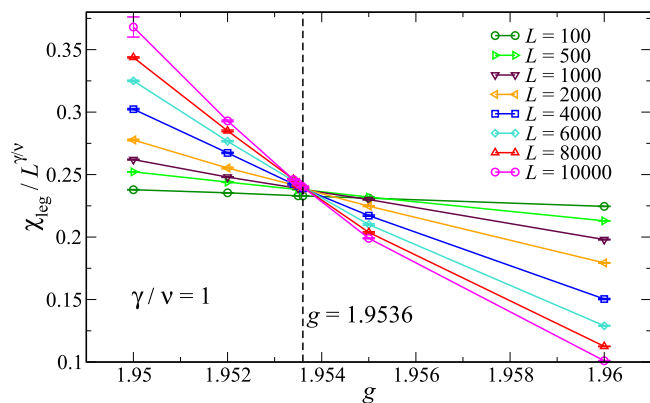
FIG. 9. Crossing point analysis of the single-leg susceptibility χ_{leg}.

FIG. 11. Data-collapse plot for the long-distance correlations $C_{L/2}$.

a corresponding data collapse plot of the data for $L > 1000$, we obtain the estimates $g_c = 1.9536(2)$ and $\nu = 1.46(2)$; cf. Fig. 10. In agreement with the above RG-based estimate ($\nu \approx 1.227$), our result for ν is larger than the mean-field value [31] $\nu_{\text{MF}} = 1$ for $\sigma = 1$. Our numerical value for ν extends beyond the RG-based estimate, which, however, was extrapolated from only the linear-order expression in ϵ. It would of course be valuable to have more accurate RG analytical estimates for ν to compare with.

To directly access the long-distance intraleg correlations, we measured in the QMC simulations the correlations between spins on the same leg at the largest accessible distances (under PBC) for a given system length L. By averaging over the values of the correlations at l distances around the maximum distance $L/2$ for a given lattice size L, we obtain a better statistics on this quantity, which we denote by $C_{L/2}$, and where we used a value of $l = 0.01L$. Based on Eq. (14) with $d = 1$, at criticality $C_{L/2}$ scales as $1/L^{z+\eta-1}$ with the system size L. A corresponding data collapse plot, using our above estimate of ν, is shown in Fig. 11, and it allows us to infer a value of $z + \eta = 1.506(7)$ and a value of $g_c = 1.9536(1)$, which matches well with the above estimate. Furthermore, we observe a corresponding crossing point in the rescaled data, cf. Fig. 12. When combined with the relation $\eta = 2 - \sigma$, we obtain from this analysis a value of $z = 0.506(7)$. Note that this result is also in accord with the overall algebraic

decay of $C(r)$ near the quantum critical point observed in Fig. 4.

We can furthermore obtain a separate estimate of the dynamical critical exponent z by performing finite-temperature simulations within the quantum critical region top $g = g_c$. This is particularly convenient since we actually use a finite-temperature QMC simulation method. In particular, we consider for this purpose the Binder ratio for the single-leg magnetic moment,

$$ B = \frac{\langle (M_{\text{leg}})^4 \rangle}{\langle (M_{\text{leg}})^2 \rangle^2}. \tag{17} $$

For finite temperatures within the quantum critical region atop the quantum critical point, this dimensionless quantify ($\phi_B = 0$) scales as

$$ B(L,T,g_c) = F_B(TL^z), \tag{18} $$

so that a corresponding data collapse plot allows us to estimate the value of z given our above estimate for g_c. Such a collapse plot for the Binder ratio is shown in Fig. 13, and we obtain from this an estimate of $z = 0.518(2)$, which agrees with the above value given the statistical uncertainty.

Finally, we examine the scaling of the spin excitation gap Δ in the quantum-disordered phase close to the quantum critical

FIG. 10. Data-collapse plot for the single-leg susceptibility χ_{leg}.
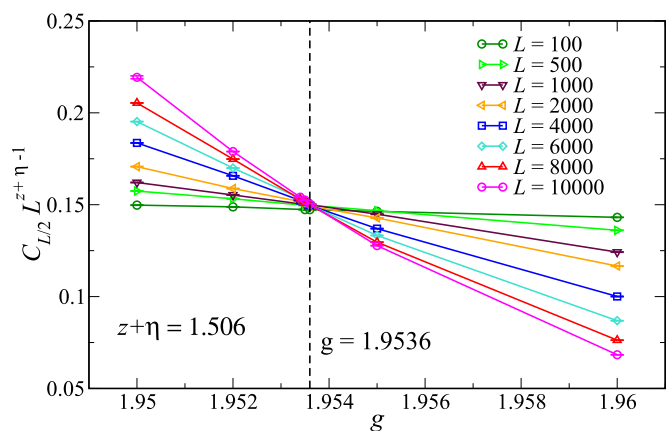
FIG. 12. Crossing point analysis of the long-distance correlations $C_{L/2}$.
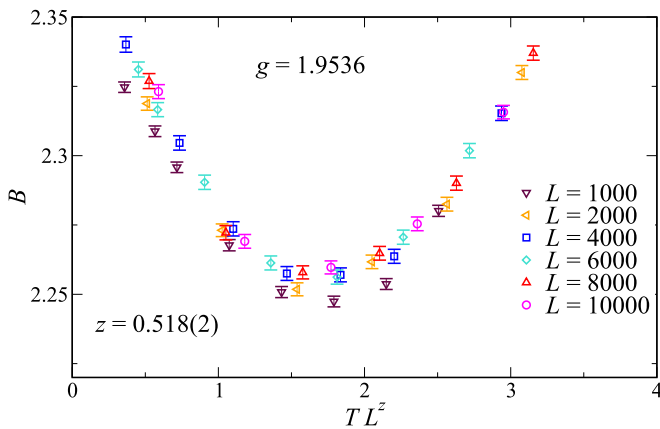
FIG. 13. Data-collapse plot for the Binder ratio B from simulations at finite temperatures atop the estimated quantum critical point.

point. We obtain an estimate for Δ from a fit of the low-temperature susceptibility χ_{uni} to the leading low-T expression for an activated behavior, $\chi_{\mathrm{uni}} \sim e^{-\Delta/T}$. We performed a linear regression of the corresponding linear temperature dependence of $-T \ln \chi_{\mathrm{uni}}$, using the data for χ_{uni} for $T < 0.02$, in order to estimate Δ for values of g close to g_c. This procedure is shown in the inset of Fig. 14, based on the $L = 8000$ data. Furthermore, near the quantum critical point, the spin gap is expected to scale as

$$\Delta \propto (g - g_c)^{z\nu}. \tag{19}$$

In the main panel of Fig. 14, we show our results for Δ in the vicinity of the quantum critical point, along with a fit to this scaling form, based on a value of $z\nu \approx 0.739$, as extracted from our above estimates for the two involved critical
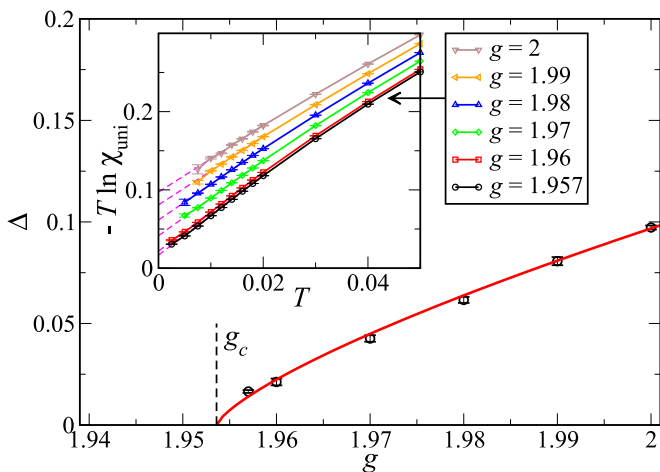

FIG. 14. Softening of the spin excitation gap Δ in the quantum disordered region near the quantum critical point. Circles are QMC estimates of the Δ, and the solid line is a fit to the quantum critical scaling form, $\Delta \propto (g - g_c)^{z\nu}$, with $z\nu = 0.739$, and $g_c = 1.9536$ (indicated by the dashed line). The inset shows the low-temperature behavior of the uniform susceptibility χ_{uni} for the $L = 8000$ system along with linear extrapolations (dashed lines) for temperatures $T < 0.02$ in order to extract the gap Δ as the extrapolated value of $-T \ln \chi_{\mathrm{uni}}$ at $T = 0$.

exponents. The scaling form fits the numerically estimated g dependence of the gap rather well. The weakly larger value of Δ extracted for the point closest to g_c, as compared to the scaling form, indicates finite-size corrections near criticality. These are anticipated, however, given that our QMC estimates for Δ are based on finite-system ($L = 8000$) data. Overall, our numerical analysis thus confirms the presence of a quantum critical point with an emerging scaling behavior for the effective spin model $\tilde{H}$, separating a gapless low-g phase from the gapped large-g quantum disordered regime.

IV. DISCUSSION

In the preceding section we observed, based on quantum Monte Carlo simulations combined with a finite-size scaling analysis, that both of the effective spin-ladder models that we considered here exhibit a quantum phase transition between a gapless, weak interleg coupling regime with a finite ferromagnetic polarization within each leg, and a gapped, strong interleg coupling quantum disordered phase. While the regime of strong interleg coupling is dominated by the formation of rung-based singlets, similar to the two-leg ladder with short-ranged interactions [23–25], the weak-coupling phase is in fact more appropriately understood in terms of two antiferromagnetically coupled superspins, each forming along one of the legs. In this sense, the basic picture of edge magnetism in graphene nanoribbons is apparently appropriate for the effective quantum spin model in the relevant parameter region for sufficiently wide zigzag nanoribbons. Note that due to the bipartite nature of the coupling geometry, Marshall's theorem implies that for any finite ladder (i.e., finite L), the ground state is a global spin singlet ($S = 0$) [37,38]. This corresponds to the fact that for any finite (zigzag) nanoribbon, the ground state within the Hubbard model description is a singlet due to Lieb's theorem [39].

There are thus two distinct phases in the thermodynamic limit, which are both in accord with the singlet nature of the finite-system ground state. The situation in the effective spin-ladder model is in fact closely related to more familiar cases such as, e.g., the Heisenberg model on the square lattice bilayer [40–46]: there, the system realizes a quantum disordered phase for strong interlayer coupling, and an antiferromagnetic phase with finite sublattice polarizations for weak interlayer coupling. However, and in contrast to the bilayer case, (i) the two polarized sublattices of the effective ladder systems considered here are well separated from each other in real space, and (ii) direct, long-ranged ferromagnetic intraleg couplings are required in order to stabilize the weak-coupling phase, given the reduced dimensionality of the effective spin-ladder systems.

We found that the coupling parameters of the effective spin-ladder model derived from the Hubbard model description for the width $W = 10$ zigzag nanoribbon [20,21] are located in the corresponding effective quantum spin model well within the weak-coupling region. The quantum disordered region is reached only upon artificially enhancing the interleg coupling beyond the quantum critical coupling strength. For even wider nanoribbons, the antiferromagnetic interleg couplings of the effective ladder model will be further reduced [20,21], so that also for such nanoribbons the effective spin model
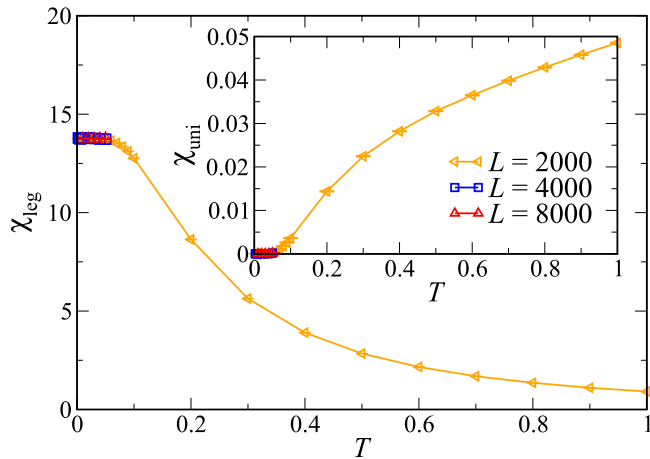
FIG. 15. Temperature dependence of the single-leg susceptibility χ_{leg} (main panel) and the uniform susceptibility χ_{uni} (inset) of the effective quantum spin model for a $W = 6$ zigzag nanoribbon at $U = t$ for different values of L.

resides within the weak-coupling regime. This is in contrast to the previously considered case of chiral nanoribbons, for which the effective spin models had a quantum disordered, spin-gapped ground state [19]. One may ask whether instead the ground states of the spin-ladder models for narrower zigzag nanoribbons, with $W < 10$, for which the antiferromagnetic interleg coupling is indeed larger, reside within the gapped, quantum disordered regime. In fact, previous numerical studies of the extremely narrow $W = 2$ zigzag nanoribbon, performed directly within the Hubbard model description, clearly identified a gapped quantum disordered ground state [15,16]. Motivated by the observation of a quantum phase transition in the effective spin models for the $W = 10$ nanoribbon, we performed quantum Monte Carlo simulations also for the effective spin-ladder model for a $W = 6$ zigzag nanoribbon (again for $U = t$), even though such a ribbon may already be too narrow for the effective spin model derivation to still be applicable [21]. For the resulting effective spin-ladder model for the $W = 6$ nanoribbon, we obtain a ratio of $J^{\text{AF}}(r = 0)/J_F = 6.141$ between the nearest-neighbor antiferromagnetic interleg coupling and the long-ranged ferromagnetic intraleg tail, which is significantly larger than the corresponding ratio of 1.95 for the $W = 10$ nanoribbon. Figure 15 shows the temperature dependence of both the uniform susceptibility and the single-leg susceptibility of the effective spin-ladder model for the $W = 6$ nanoribbon as obtained from the QMC simulations, exhibiting that this

effective spin-ladder model indeed has a gapped, quantum disordered ground state. From the temperature dependence of the uniform susceptibility, we estimate a corresponding spin gap of $\Delta \approx 0.3 \, J^{\text{F}}(1) = 0.014t$, in terms of the Hubbard model hopping strength (we also considered explicitly the case of $W = 8$, for which we find the ground state to be located within the gapless, weak-coupling region). Even though the truncated effective spin model derivation will be less accurate for such a narrow ribbon, the above result shows that indeed both phases may in principle be accessed in effective spin-ladder models for zigzag graphene nanoribbons.

Anticipating the fact that the effective quantum spin models describe the correlations among the edge magnetic moments in graphene nanoribbons within a controlled but nevertheless approximate framework, we are not in a position to discern, based on our findings, whether edge magnetism is indeed stabilized in wide graphene zigzag nanoribbons, at least in the ground state. For this purpose, various additional effects may also have to be considered, such as electronic interactions beyond the local Hubbard repulsion [10], extended hopping terms in the kinetic energy, as well as exchange anisotropies deriving, e.g., from graphene-to-substrate couplings [47]. The above findings nevertheless represent a plausible scenario for stable edge magnetism on wider zigzag nanoribbons, at least within the effective spin model for the most basic Hubbard model description. It would be worthwhile to extend beyond our investigation toward analyzing also the low-energy spin dynamics and its evolution across the quantum phase transition, which is feasible, e.g., with quantum Monte Carlo methods. Moreover, the real-time out-of-equilibrium behavior of such effective spin models with long-ranged interactions can be probed in order to examine the quantum nature of the spin response, and the evolution of the relevant time scales of the magnetic fluctuations [19] both within the weak-coupling regime as well as upon crossing the quantum critical point. Such a study could be performed using advanced numerical methods for quantum systems with long-ranged interactions [48], and this is also left for future investigations.

[1] M. Fujita, K. Wakabayashi, K. Nakada, and K. Kusakabe, J. Phys. Soc. Jpn. **65**, 1920 (1996).

[2] A. H. Castro Neto, N. M. R. Peres, K. S. Novoselov, and A. K. Geim, Rev. Mod. Phys. **81**, 109 (2009).

[3] K. Wakabayashi, M. Sigrist, and M. Fujita, J. Phys. Soc. Jpn. **67**, 2089 (1998).

[4] Y.-W. Son, M. L. Cohen, and S. G. Louie, Nature (London) **444**, 347 (2006).

[5] L. Pisani, J. A. Chan, B. Montanari, and N. M. Harrison, Phys. Rev. B **75**, 064418 (2007).

[6] O. V. Yazyev and M. I. Katsnelson, Phys. Rev. Lett. **100**, 047209 (2008).

[7] O. V. Yazyev, Rep. Prog. Phys. **73**, 056501 (2010).

[8] J. Jung, Phys. Rev. B **83**, 165415 (2011).

[9] H. Karimi and I. Affleck, Phys. Rev. B **86**, 115446 (2012).

[10] Z. Shi and I. Affleck, Phys. Rev. B **95**, 195420 (2017).

[11] C. Tao *et al.*, Nat. Phys. **7**, 616 (2011).

[12] G. Z. Magda *et al.*, Nature (London) **514**, 608 (2014).

[13] T. L. Makarova *et al.*, Sci. Rep. **5**, 13382 (2015).

[14] P. Ruffieux *et al.*, Nature (London) **531**, 489 (2016).

[15] T. Hikihara, X. Hu, H.-H. Lin, and C.-Y. Mou, Phys. Rev. B **68**, 035432 (2003).

[16] H. Feldner, Z. Y. Meng, T. C. Lang, F. F. Assaad, S. Wessel, and A. Honecker, Phys. Rev. Lett. **106**, 226401 (2011).

[17] M. Golor, C. Koop, T. C. Lang, S. Wessel, and M. J. Schmidt, Phys. Rev. Lett. **111**, 085504 (2013).

[18] M. Golor, T. C. Lang, and S. Wessel, Phys. Rev. B **87**, 155441 (2013).

[19] M. Golor, S. Wessel, and M. J. Schmidt, Phys. Rev. Lett. **112**, 046601 (2014).

[20] M. J. Schmidt, M. Golor, T. C. Lang, and S. Wessel, Phys. Rev. B **87**, 245431 (2013).

[21] C. Koop and M. J. Schmidt, Phys. Rev. B **92**, 125416 (2015).

[22] H. Yoshioka, J. Phys. Soc. Jpn. **72**, 2145 (2003).

[23] M. Roji and S. Miyashita, J. Phys. Soc. Jpn. **65**, 883 (1996).

[24] A. K. Kolezhuk and H.-J. Mikeska, Phys. Rev. B **53**, R8848(R) (1996).

[25] T. Vekua, G. I. Japaridze, and H.-J. Mikeska, Phys. Rev. B **67**, 064419 (2003).

[26] A. W. Sandvik, Phys. Rev. E **68**, 056701 (2003).

[27] K. Fukui and S. Todo, J. Comput. Phys. **228**, 2629 (2009).

[28] F. D. M. Haldane, Phys. Rev. Lett. **60**, 635 (1988).

[29] B. S. Shastry, Phys. Rev. Lett. **60**, 639 (1988).

[30] F. D. M. Haldane, Phys. Rev. Lett. **66**, 1529 (1991).

[31] A. Dutta and J. K. Bhattacharjee, Phys. Rev. B **64**, 184106 (2001).

[32] M. F. Maghrebi, Z.-X. Gong, M. Foss-Feig, and A. V. Gorshkov, Phys. Rev. B **93**, 125128 (2016).

[33] N. Defenu, A. Trombettoni, and S. Ruffo, Phys. Rev. B **96**, 104432 (2017).

[34] O. N. Vassiliev, I. V. Rojdestvenski, and M. G. Cottam, Physica A **294**, 139 (2001).

[35] S. Sachdev, *Quantum Phase Transitions* (Cambridge University Press, Cambridge, 2011).

[36] S. Pankov, S. Florens, A. Georges, G. Kotliar, and S. Sachdev, Phys. Rev. B **69**, 054426 (2004).

[37] W. Marshall, Proc. R. Soc. London, Ser. A **232**, 48 (1955).

[38] E. Lieb and D. Mattis, J. Math. Phys. **3**, 749 (1962).

[39] E. Lieb, Phys. Rev. Lett. **62**, 1201 (1989).

[40] R. R. P. Singh, M. P. Gelfand, and D. A. Huse, Phys. Rev. Lett. **61**, 2484 (1988).

[41] A. J. Millis and H. Monien, Phys. Rev. Lett. **71**, 210 (1993).

[42] A. J. Millis and H. Monien, Phys. Rev. B **50**, 16606 (1994).

[43] A. W. Sandvik and D. J. Scalapino, Phys. Rev. Lett. **72**, 2777 (1994).

[44] A. V. Chubukov and D. K. Morr, Phys. Rev. B **52**, 3521 (1995).

[45] T. Sommer, M. Vojta, and K. W. Becker, Eur. Phys. J. B **23**, 329 (2001).

[46] L. Wang, K. S. D. Beach, and A. W. Sandvik, Phys. Rev. B **73**, 014431 (2006).

[47] W. Zhang, F. Hajiheidari, Y. Li, and R. Mazzarello, Nat. Sci. Rep. **6**, 29009 (2016).

[48] M. P. Zaletel, R. S. K. Mong, C. Karrasch, J. E. Moore, and F. Pollmann, Phys. Rev. B **91**, 165112 (2015).